JACS
JOURNAL OF THE AMERICAN CHEMICAL SOCIETY
pubs.acs.org/JACS
Article

# Dibenzocyclooctyne Conjugation Enhances Antigen Cross-Presentation and T-Cell Killing for Potent Cancer Vaccines

Zhiguo Li,[§] Tengyao Wang,[§] Weifan Li,[§] Peiyu Yu, Kangxiu Wu, Chanjuan Su, Fuxiang Wang, Huosheng Zhou, Fan Lan, Yaofeng Zhou, Kaimin Cai, Menghua Xiong, Songyin Huang, Jianjun Cheng,* Minmin Xiong,* Kaiting Yang,* and Yan Bao*

Cite This: *J. Am. Chem. Soc.* 2026, 148, 8223–8235
Read Online



**ABSTRACT:** Cancer vaccines have gained considerable attention for tumor prevention and therapy; however, their clinical efficacy remains limited by insufficient activation of antigen-specific cytotoxic T lymphocytes (CTLs). This limitation is primarily due to the inability of conventional vaccine components to effectively promote dendritic-cell-mediated cross-presentation and activation. While adjuvants are often used to enhance this interaction, many conventional adjuvants suffer from poor biocompatibility and systemic toxicity, limiting their clinical utility. Here, we report a vaccine strategy that leverages the bioorthogonal click chemistry reagent dibenzocyclooctyne (DBCO) as an adjuvant-like immune enhancer to promote cross-presentation and a CTL response. DBCO modification to antigen significantly increased antigen uptake by dendritic cells *in vitro* and promoted MHC class I-mediated cross-presentation via activation of the NF-κB/iNOS signaling pathway. In murine tumor models, systemic administration of DBCO-conjugated protein vaccines elicited enhanced $CD8^+$ T-cell activation, leading to improved tumor control and long-term immune memory. Furthermore, DBCO-modified protein vaccines significantly suppressed tumor metastasis when combined with anti-PD-1 treatment. Collectively, our findings extend the immunotherapeutic potential of click chemistry reagents and establish a promising platform for enhancing CTL-mediated cancer vaccine efficacy in clinical settings.

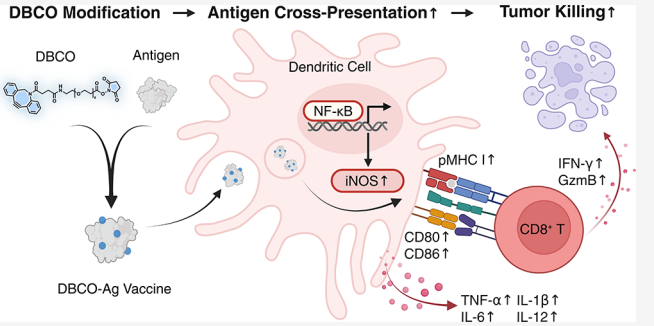




## INTRODUCTION

Cancer immunotherapy has emerged as a promising approach to harnessing the host immune system to target and eliminate established tumors. Among the various strategies, therapeutic cancer vaccines aim to induce potent immune responses against tumor-associated or tumor-specific antigens.[1] Discovery of tumor neoantigens offers a highly specific target for immune recognition and has been associated with durable responses in both preclinical models and early-phase clinical trials.[2] However, clinical translation remains limited by inefficient antigen delivery, poor uptake by antigen-presenting cells (APCs), and inadequate cytotoxic T lymphocyte (CTL) activation.[3−6] These challenges are particularly pronounced in the context of metastatic disease, where immunosuppression limits vaccine efficacy.

CTLs mediate targeted cell killing through MHC class I (MHC I)-restricted antigen presentation,[7,8] making them particularly effective in preventing tumor relapse and controlling tumor progression. Dendritic cells (DCs) are central to initiating effective antitumor immunity, but efficient *in vivo* antigen delivery to DCs remains a critical bottleneck. A variety of approaches, including nanoparticle-based delivery systems, DC-targeting ligands, and cell-based platforms, have been developed to address this issue.[9] However, these methods often involve relatively complex formulations, which could pose challenges in terms of their toxicity and clinical translatability. Traditional adjuvants, such as aluminum salts (alum), Freund's adjuvant, and MF59, primarily enhance humoral immune responses by facilitating antigen interaction with B cells and promoting Th2 responses.[10−12] While these adjuvants can activate innate immune pathways, they have limited ability to induce cross-presentation and CTL activation, which are critical for effective cancer immunotherapy. In recent years, a new generation of adjuvants, comprising immune receptor agonists, immunoregulatory molecules, and nanoparticle-based systems, has shown promise in improving antigen cross-presentation, enhancing MHC I expression, and potentiating CTL activation. However, challenges such as

**Received:** October 5, 2025
**Revised:** February 3, 2026
**Accepted:** February 5, 2026
**Published:** February 17, 2026

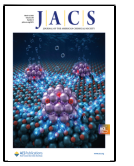





https://doi.org/10.1021/jacs.5c17189
*J. Am. Chem. Soc.* 2026, 148, 8223−8235

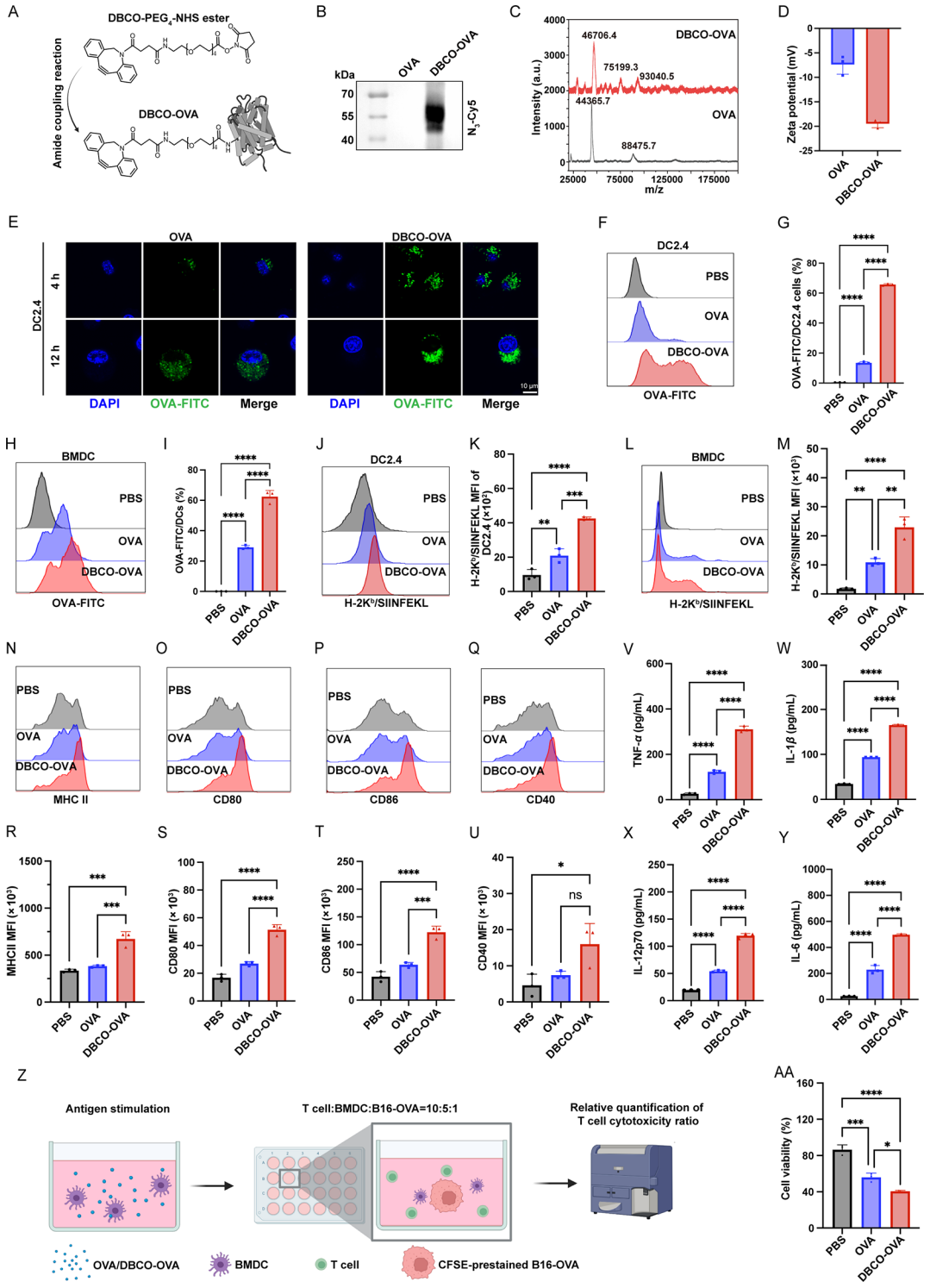


**Figure 1.** DBCO conjugation enhances antigen uptake and promotes MHC I-mediated cross-presentation. (A) Schematic representation of the amide coupling reaction between DBCO-PEG$_4$-NHS ester and DBCO-conjugated OVA (DBCO-OVA). (B) Western blot analysis confirming the successful conjugation of DBCO to OVA. (C) MALDI-TOF mass spectra of OVA and DBCO-OVA. (D) Zeta potential analysis comparing OVA and DBCO-OVA. (E) Confocal microscopy images demonstrating enhanced uptake of DBCO-OVA by DC2.4 cells, bar = 10 $\mu$m. (F–I) Flow cytometry analysis showing increased uptake of DBCO-OVA by DC2.4 cells (F, G) and BMDCs (H, I). (J–M) Flow cytometry analysis illustrating that DBCO-OVA treatment enhanced H-2K$^b$-SIINFEKL presentation on the surface of DC2.4 cells (J, K) and BMDCs (L, M) compared to that of OVA. (N–U) Flow cytometry analysis of surface maturation markers (MHC II, CD80, CD86, and CD40) on BMDCs following OVA or DBCO-OVA treatment. (V–Y) ELISA quantification of cytokine (TNF-$\alpha$, IL-1$\beta$, IL-12p70, and IL-6) concentrations in the culture supernatants of BMDCs stimulated with DBCO-OVA or OVA. (Z and AA) Flow cytometry analysis assessing T cell-mediated cytotoxicity, in which CFSE-labeled B16-OVA cells were cocultured with CD8$^+$ T cells and BMDCs pulsed with DBCO-OVA or OVA (T:BMDC:16-OVA = 10:5:1). (D, G, I, K, M, R–Y, and AA) $n$ = 3 biologically independent samples. (E) Representative images from three independent experiments are shown. Statistical analysis was performed using one-way analysis of variance (ANOVA), and the data are presented as mean ± standard deviation (SD). $^{**}P < 0.01$; $^{***}P < 0.001$; $^{****}P < 0.0001$. Panel Z created with BioRender.com.



https://doi.org/10.1021/jacs.5c17189
J. Am. Chem. Soc. 2026, 148, 8223–8235

excessive innate immune activation, systemic toxicity, and manufacturing complexities remain.[13−15]

Dibenzocyclooctyne (DBCO), a key reagent in copper-free click chemistry, has gained attention in drug conjugation, cell labeling, and targeted drug delivery due to its rapid reactivity and compatibility with physiological conditions.[16−18] Unlike conventional copper-catalyzed click reactions, DBCO-mediated click reactions eliminate the need for cytotoxic copper catalysts, making them particularly attractive for biological and clinical uses. Previous studies have primarily employed DBCO for surface modification of cells or for constructing bioorthogonal click chemistry-mediated target drug delivery systems.[19,20] However, the immunomodulatory effect of direct DBCO modification has not been previously reported.

In this study, we report a novel protein vaccine strategy based on conjugation of DBCO to tumor-associated antigen. We show that DBCO−antigen conjugation markedly promotes antigen uptake by APCs and improves antigen cross-presentation, consequently augmenting effector T cell cytotoxicity and memory. Using a B16-OVA lung metastasis model, we show that the DBCO-conjugated vaccine suppresses tumor burden, prolongs survival, and synergizes with the immune checkpoint blockade (ICB). Importantly, our data reveal that DBCO modification enables local immune priming in metastatic niches by enhancing DC and T-cell recruitment and activation. These results uncover an unexpected immunomodulatory role for DBCO and highlight its potential as a bioorthogonal immune potentiator in cancer vaccine design.

## RESULTS

### DBCO Conjugation Enhances Antigen Uptake and Promotes MHC I-Mediated Cross-Presentation

Protein-based vaccines usually contain multiple lysine residues, with exposed $\epsilon$-amino groups that can efficiently undergo covalent conjugation with *N*-hydroxysuccinimide (NHS) esters. To establish a modular and generalized strategy for antigen loading, we utilized DBCO-$PEG_4$-NHS to modify the model antigen ovalbumin (OVA), yielding DBCO-conjugated OVA (DBCO-OVA) (Figure 1A). Western blot analysis demonstrated that DBCO-OVA efficiently reacted with an azide-functionalized Cy5 ($N_3$-Cy5) via strain-promoted azide−alkyne cycloaddition (SPAAC), confirming the successful DBCO functionalization of the protein (Figure 1B). MALDI-TOF mass spectrometry indicated an average of ∼4 DBCO groups conjugated per molecule of the OVA (Figure 1C).

High-resolution liquid chromatography-tandem mass spectrometry (LC-MS/MS) was employed to identify the DBCO conjugation sites on the OVA. As detailed in Table S1, DBCO conjugation occurs randomly on lysines. To assess whether DBCO conjugation alters the global folding of the antigen, we performed circular dichroism (CD) spectroscopy, which showed that DBCO-OVA exhibited a secondary structure similar to that of native OVA (Figure S2A). Quantitative analysis revealed similar content of $\alpha$-helix (15 vs 18%) or $\beta$-sheet (35 vs 32%) between the conjugated and native proteins (Figure S2B). This indicates that DBCO modification does not disrupt the overall folding of OVA. DBCO−antigen conjugation increased the protein's negative surface charge, as evidenced by the zeta potential decreasing from −7.39 to −19.47 mV (Figure 1D).

Next, we evaluated the uptake of DBCO-modified antigens by DCs. DBCO-OVA and unmodified OVA were fluorescently labeled with FITC and incubated with DC2.4 cells. Confocal microscopy showed significantly stronger intracellular fluorescence in DBCO-OVA-treated cells than in controls (Figure 1E), indicating an enhanced antigen uptake. This observation was further confirmed by flow cytometry, which showed a substantial increase in the proportion of antigen-positive DC2.4 cells, from 13.4% in the OVA group to 65.7% in the DBCO-OVA group, representing nearly a 5-fold enhancement (Figure 1F,G). Consistent results were obtained using bone-marrow-derived dendritic cells (BMDCs), where DBCO modification to OVA increased antigen uptake efficiency from 29.0 to 62.4%, demonstrating the enhancement across different DC models (Figure 1H,I).

To determine whether modification of DBCO to antigen enhances its cross-presentation through MHC I molecules, we quantified the surface expression of H-$2K^b$/SIINFEKL complexes on DCs. In DC2.4 cells, DBCO-OVA treatment increased the mean fluorescence intensity (MFI) of H-$2K^b$/SIINFEKL from 2092.7 to 4255.1 (Figure 1J,K). Similarly, in BMDCs, MFI rose from 10,898.5 to 22,939.5 (Figure 1L,M). These findings indicate that modification of the DBCO to antigen significantly improves antigen processing and MHC I loading efficiency, thereby enhancing the cross-presentation capability of DCs. Beyond enhancing antigen presentation, the DBCO-modified antigen also promoted DC maturation. Flow cytometry analysis revealed that DBCO-OVA-treated BMDCs exhibited significantly elevated the surface expression of costimulatory molecules (CD80, CD86, and CD40) and MHC II compared to those from the control group (Figure 1N−U). ELISA further demonstrated that DBCO-OVA stimulated secretion of pro-inflammatory cytokines, such as TNF-$\alpha$, IL-1$\beta$, IL-12p70, and IL-6, indicating enhanced DC activation (Figure 1V−Y). We further evaluated the T-cell response induced by DCs using an *in vitro* T-cell killing assay. Antigen-pulsed BMDCs were cocultured with $CD8^+$ T cells, and CFSE-labeled B16-OVA cells were used as target cells. Flow cytometry indicated significantly reduced tumor cell survival in the DBCO-OVA group, with an approximately 15.2% increase in killing efficiency (Figure 1Z,AA). These findings indicate that DBCO modification to OVA not only enhances antigen uptake and presentation but also effectively improves the effector function of CTLs. Notably, direct addition of OVA and DBCO-$PEG_4$-NHS into the cell culture medium failed to replicate these effects, i.e., no enhanced antigen uptake, presentation, or DC maturation (Figure S3). These results indicate that DBCO-$PEG_4$-NHS alone does not possess intrinsic adjuvant properties and that covalent conjugation is essential for its immunostimulatory function.

To exclude the possibility that the observed immunostimulatory effects were caused by nonspecific physicochemical alterations, we synthesized and evaluated a series of structurally defined control analogs (Figure S4), including (1) DBCO-$PEG_4$-COOH + OVA, a physical mixture control where the free DBCO ligand was simply mixed with the antigen without covalent attachment; (2) m-$PEG_4$-OVA, a PEG-only control to rule out PEGylation effects; (3) BCN-OVA, modified with bicyclononyne, an alternative strained alkyne; and (4) THDBCO-OVA, modified with a nonstrained dibenzocyclooctene analog retaining the exact hydrophobic aromatic scaffold of DBCO but with a reduced (nonalkyne) bond. We assessed DC antigen cross-presentation and maturation following


https://doi.org/10.1021/jacs.5c17189
J. Am. Chem. Soc. 2026, 148, 8223−8235

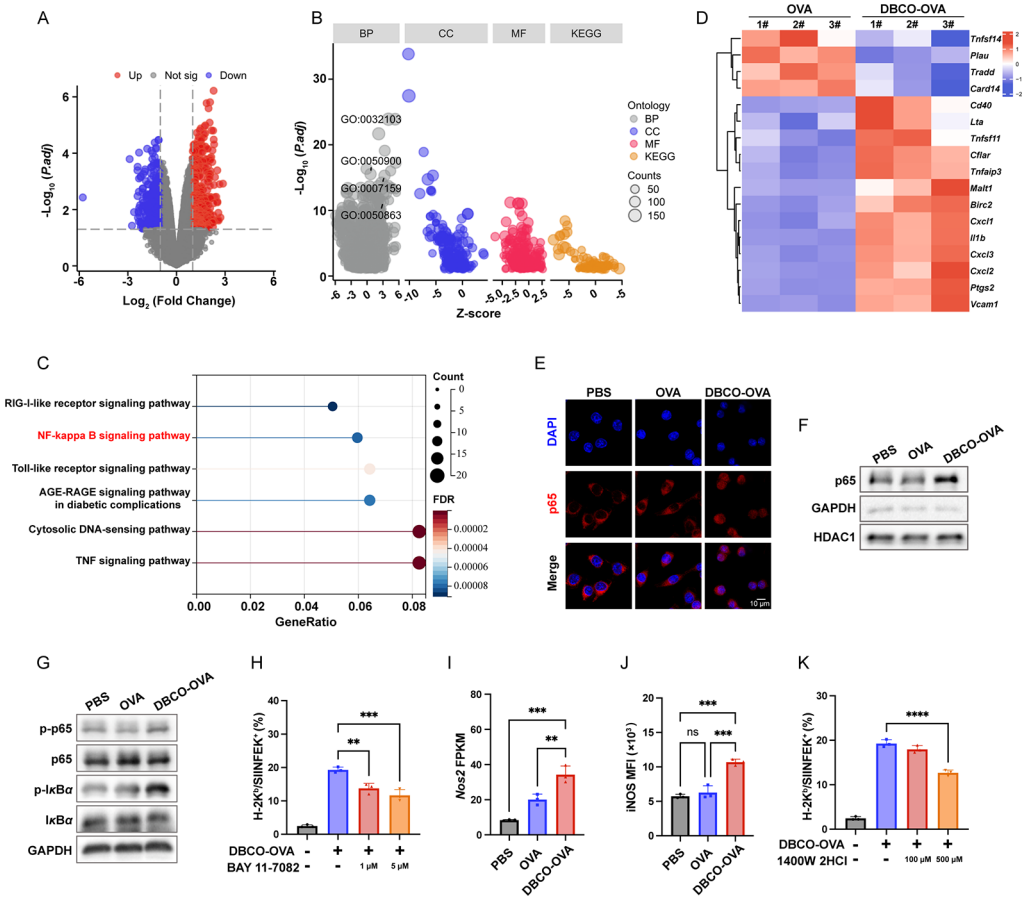


**Figure 2.** Transcriptomic analysis of BMDCs stimulated with OVA or DBCO-OVA. (A) Volcano plots showing differentially expressed genes in BMDCs stimulated with OVA or DBCO-OVA, where genes with a *P*-value <0.05 and $|\log_2(\text{fold change})| > 0.58$ are considered significantly different. (B) Gene Ontology (GO) and KEGG enrichment analysis of differentially expressed gene ($P < 0.05$). (C) KEGG pathway enrichment analysis of differentially expressed genes, highlighting the top 6 signaling pathways of interest in a bubble plot ($P < 0.05$). (D) Heatmap displaying the differential expression of genes in the NF-κB signaling pathway in response to OVA and DBCO-OVA stimulation. (E) Immunofluorescence images showing nuclear translocation of p65 following OVA or DBCO-OVA stimulation, indicating activation of the NF-κB pathway. (F) Western blot analysis confirming p65 nuclear translocation after DBCO-OVA stimulation. (G) Western blot analysis of p65 and IκBα phosphorylation in BMDCs cocultured with 50 μg of OVA and DBCO-OVA, for 24 h. (H) H-2K$^b$-SIINFEKL complex levels on BMDCs at 24 h post DBCO-OVA plus the NF-κB inhibitor BAY 11−7082 (1 μM or 5 μM) treatment. (I) *Nos2* expression level in BMDCs 24 h post DBCO-OVA treatment. (J) iNOS level in BMDCs treated with DBCO-OVA detected by flow cytometry. (K) H-2K$^b$-SIINFEKL complex levels on BMDCs at 24 h post DBCO-OVA plus the iNOS inhibitor 1400W 2HCl (100 or 500 μM) treatment. (D, H−K) $n = 3$ biologically independent samples. (E−G) Representative images from three independent experiments are shown. Statistical analysis was performed using one-way ANOVA, and the data are presented as the mean ± SD. $^{**}P < 0.01$; $^{***}P < 0.001$; $^{****}P < 0.0001$.

treatment with these conjugates. As shown in Figure S4D−F, the DBCO-OVA conjugate induced significantly enhanced antigen cross-presentation and upregulation of CD80 and CD86 compared to all tested structural analog controls. The nonstrained analog (THDBCO-OVA), the alternative strained alkyne (BCN-OVA), the PEG-only conjugate (m-PEG$_4$-OVA), and the physical mixture control all exhibited basal levels of DC activation and MHC I presentation comparable to unmodified OVA controls. These results indicate that the adjuvant-like activity was not attributable to nonspecific alterations such as PEGylation, surface charge, hydrophobic aromatic scaffolds, or the presence of a strained alkyne alone.

To investigate whether DBCO modification on the antigen epitope could influence its interaction with the MHC I molecule, we performed a molecular docking method using the H-2K$^b$ molecule with either the native SIINFEKL peptide or the DBCO-SIINFEKL conjugate. As illustrated in Figure S5, the analysis suggested that the predicted binding free energy of the DBCO-modified epitope (−7.444 ± 0.260 kcal/mol) was comparable to that of the native SIINFEKL peptide (−7.944 ± 0.508 kcal/mol). These results indicate that DBCO modification does not compromise the affinity of the peptide−MHC I complex, suggesting that the enhanced cross-presentation is unlikely to arise from altered peptide−MHC physical interactions but instead reflects the adjuvant-like immunostimulatory effects associated with DBCO modification.

Considering the heterogeneity of cancers and the challenges of recognizing tumor-specific antigens, we extended this strategy to tumor cell lysates (TCL) to explore the broader applicability of DBCO modification. DBCO-TCL again significantly enhanced BMDC uptake, with the uptake rate increasing from 58.1 to 73.4% (Figure S6). Furthermore, DBCO-modified TCL significantly promoted DC maturation, as evidenced by upregulated expression of costimulatory molecules, CD80 (MFI from 23,194.3 to 39,816.5) and CD40 (MFI from 23,286 to 38,564.7), representing more than a 50% increase in both markers. These demonstrate that


https://doi.org/10.1021/jacs.5c17189
J. Am. Chem. Soc. 2026, 148, 8223−8235

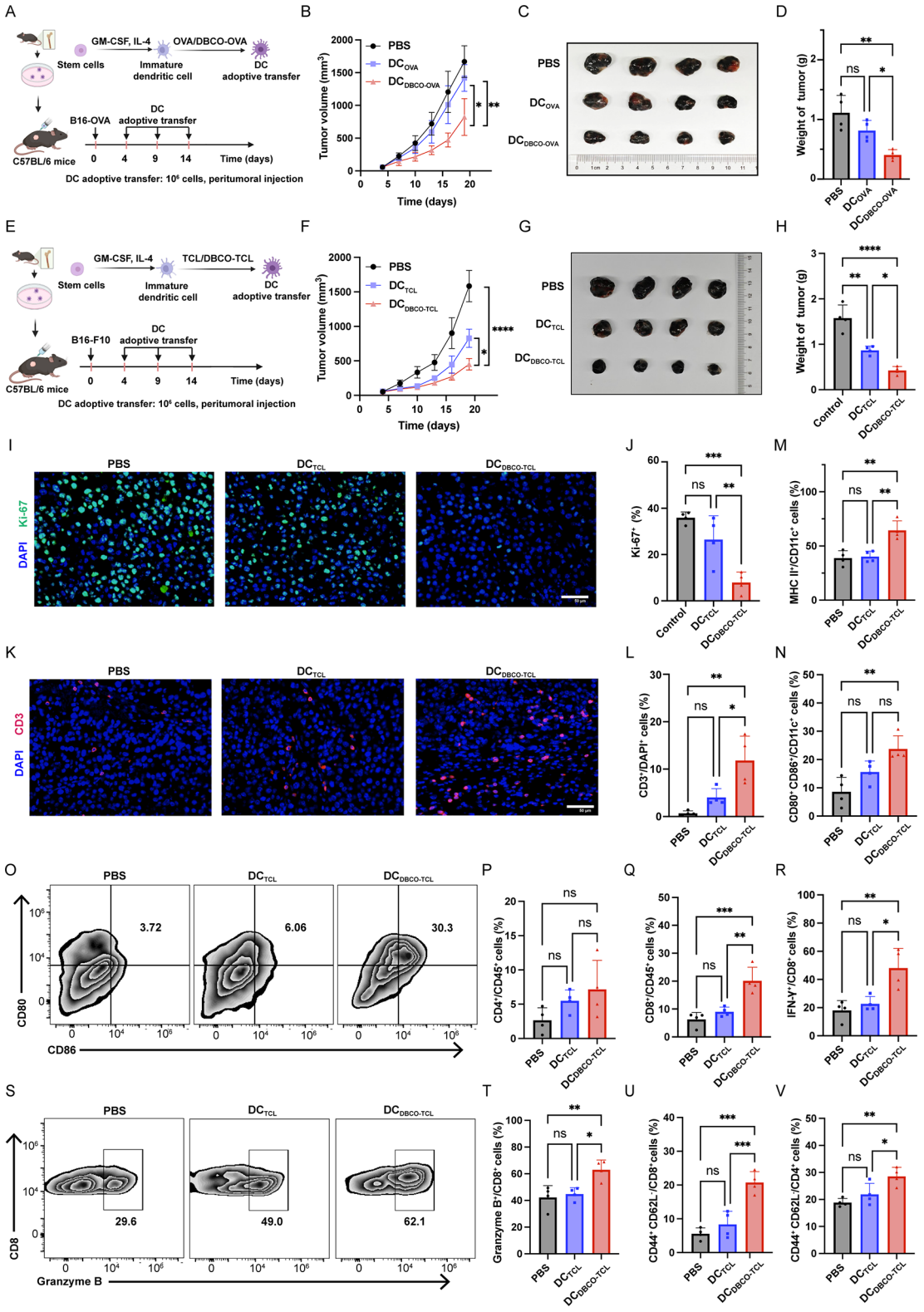


**Figure 3.** DBCO-modified antigens enhance the antitumor immune response of DCs. (A) Workflow for adoptive transfer of DCs into B16-OVA tumor-bearing mice. BMDCs were generated with GM-CSF and IL-4 before being pulsed ex vivo with either OVA alone or DBCO-OVA and then injected subcutaneously adjacent to established B16-OVA tumors on days 4, 9, and 14 post-tumor inoculation. (B) Tumor growth curves showing the effect of DC (pulsed with OVA or DBCO-OVA) adoptive transfer on tumor progression in the B16-OVA model ($n$ = 4 mice/group). (C) Image of tumors at the end point of the experiment on day 19. (D) Tumor weight measurements on day 19 after treatment. (E) Workflow for adoptive transfer of DCs into B16−F10 tumor-bearing mice. BMDCs were generated with GM-CSF and IL-4 before being pulsed ex vivo with either B16-F10 TCL or DBCO-TCL and then injected subcutaneously adjacent to established B16-F10 tumors on days 4, 9, and 14 post-tumor inoculation. (F) Tumor growth curves of B16-F10 tumors, illustrating the therapeutic effect of DC (pulsed with TCL or DBCO-TCL) adoptive transfer ($n$ = 4 mice/group). (G) Image of dissected B16-F10 tumors on day 19. (H) Tumor weight measurements for B16-F10 tumors on day 19.



https://doi.org/10.1021/jacs.5c17189
J. Am. Chem. Soc. 2026, 148, 8223−8235

**Figure** 3. continued

(I) Ki-67 immunofluorescence staining of tumor sections from B16-F10 tumors after the DC adoptive transfer treatment. Bar = 50 $\mu$m. (J) Quantification of the percentage of Ki-67$^+$ cells. (K) CD3 immunofluorescence staining of tumor sections from B16-F10 tumors after DC adoptive transfer treatment. Bar = 50 $\mu$m. (L) Quantification of the percentage of CD3$^+$ T cells in tumor sections. (M) Percentages of MHC II$^+$ of CD11c$^+$ DCs in B16-F10 tumor tissues on day 19 post-treatment. (N, O) Quantification and representative flow cytometry plots showing the percentages of mature DCs (CD80$^+$CD86$^+$) in B16-F10 tumor tissues on day 19 post-treatment. (P) Quantification of CD4$^+$ T cells in B16-F10 tumor tissues on day 19 post-treatment. (Q) Quantification of CD8$^+$ T cells in B16-F10 tumor tissues on day 19 post-treatment. (R, S) Quantification and representative flow cytometry plots of IFN-$\gamma^+$ T cells in B16-F10 tumor tissues on day 19 post-treatment. (T) Quantification of granzyme B$^+$ T cells in B16-F10 tumor tissues on day 19 post-treatment. (U, V) Percentages of effector memory T cells (CD44$^+$CD62L$^-$) of CD8$^+$ T cells and CD4$^+$ T cells in spleens on day 19 post-treatment. Tumor growth curves over time were analyzed using ordinary two-way ANOVA, while other data were analyzed using one-way ANOVA. The data are presented as the mean ± SD. $n$ = 4 mice/group. In parts (I) and (K), representative images from three independent experiments are shown. ns, no significance; *$P$ < 0.05; **$P$ < 0.01; ***$P$ < 0.001; ****$P$ < 0.0001. Panels A and E created with BioRender.com.

DBCO can serve as a broadly applicable modification strategy to enhance the immunogenicity of structurally diverse antigen preparations.

## DBCO-Antigen Vaccine Improves DC Function via the NF-κB/iNOS Signaling Axis

To understand the molecular mechanism through which DBCO modification enhances the antigen presentation, we performed RNA sequencing analysis of BMDCs treated with PBS, OVA, or DBCO-OVA. Here, PBS served as a negative control to show baseline gene expression, while OVA represented the unmodified antigen, allowing for the distinction between antigen-specific and DBCO-specific effects. Comparing the DBCO-OVA to PBS group identified global transcriptional changes induced by DBCO-OVA, where 1189 genes were upregulated and 1524 genes were downregulated ($|\log_2(\text{fold change})| > 0.58$, $P < 0.05$) (Figure S7). Comparing the DBCO-OVA to OVA group further isolated the specific effects induced by DBCO modification, where 826 genes were upregulated and 1354 genes were downregulated ($|\log_2(\text{fold change})| > 0.58$, $P < 0.05$) (Figure 2A). Furthermore, we compared gene expression profiles of BMDCs treated with OVA and DBCO-OVA to identify genes specifically regulated by DBCO modification independent of the antigen itself. Gene Ontology (GO) analysis indicated enrichment of immune-related pathways, including leukocyte cell−cell adhesion (GO:0007159), leukocyte migration (GO:0050900), and positive regulation of response to external stimulus (GO:0032103) and regulation of T-cell activation (GO:0050863) (Figure S7B and Figure 2B). KEGG pathway enrichment analysis further identified the activation of immune regulatory networks, including NF-κB, TNF, Toll-like receptor, and RIG-I-like receptor signaling pathways in DBCO-OVA-treated BMDCs (Figure 2C). These results suggest that DBCO modification to antigen engages key innate immune pathways to enhance DC activation.

Given the critical role of the NF-κB signaling pathway in regulating pro-inflammatory cytokine production, costimulatory molecule, and MHC upregulation,[21] we further investigated its activation in response to DBCO-conjugated antigens. A heatmap of NF-κB pathway genes revealed significant upregulation of several key genes, including chemokines such as *Cxcl1* and *Cxcl2*, and the pro-inflammatory cytokine *Il1b*, in BMDCs treated with DBCO-OVA versus OVA (Figure 2D). Immunofluorescence analysis showed that DBCO-OVA treatment promoted the translocation of the p65 subunit from the cytoplasm to the nucleus (Figure 2E), consistent with the results of Western blot analysis (Figure 2F), indicating the activation of the canonical NF-κB pathway. This was further confirmed by Western blot analysis, which showed an increased level of phosphorylation of p65 and its inhibitory protein IκBα in the DBCO-OVA-treated group (Figure 2G). To determine the functional importance of NF-κB activation, we treated DCs with a selective NF-κB inhibitor BAY 11-7082 during antigen loading. The results demonstrated that blocking NF-κB signaling significantly reduced the antigen-presenting capacity induced by DBCO-OVA (Figure 2H), confirming the crucial role of the NF-κB pathway in DBCO-mediated immunostimulation. Additionally, bulk RNA-seq analysis revealed a significant upregulation of inducible nitric oxide synthase (iNOS, encoded by *Nos2*) in DBCO-OVA-treated cells (Figure 2I), which is a downstream effector of NF-κB.[22−24] Flow cytometry further validated an approximately 1.7-fold increase in iNOS protein levels in DBCO-OVA-treated DCs (Figure 2J). Functionally, pharmacological inhibition of iNOS using 1400W 2HCl significantly impaired DBCO-OVA-mediated antigen presentation (Figure 2K), supporting a critical role for the NF-κB/iNOS axis in promoting DC function. Together, the DBCO-modified antigen systematically enhances DC antigen processing and cross-presentation by activating the NF-κB/iNOS signaling pathway.

## DCs Treated with DBCO-Antigen Vaccine Suppress Tumor Growth in Mouse Models

Next, we sought to determine whether DBCO modification of antigens enhances the role of DC in antitumor immunity. We pulsed DCs with an OVA or DBCO-OVA before adoptively transferring them to B16-OVA tumor-bearing mice. Mice received three peritumoral injection of DBCO-OVA-pulsed DCs on days 4, 9, and 14 post-tumor inoculation (Figure 3A). Compared with PBS or OVA-treated DC groups, mice receiving DBCO-OVA-treated DCs exhibited significantly reduced tumor growth, suggesting that DBCO-enhanced DC activation contributes to tumor control (Figure 3B). Terminal dissection confirmed that the DBCO-OVA-treated DC group had markedly lower tumor weights (Figure 3C,D), confirming the enhanced antitumor activity of this modification strategy. Additionally, no significant differences in body weight were observed across the groups (Figure S8A).

To validate this approach in a more complicated antigen context, we utilized DBCO-TCL (Figure 3E). The DBCO-TCL-pulsed DCs exhibited superior tumor suppression, showing 71.5% tumor volume inhibition, a 23.7% improvement over unmodified TCL (Figure 3F). End point tumor weights further supported these findings (Figure 3G,H). Again, there were no significant changes in body weight across the groups, indicating a favorable biocompatibility (Figure S8B).



https://doi.org/10.1021/jacs.5c17189
J. Am. Chem. Soc. 2026, 148, 8223−8235

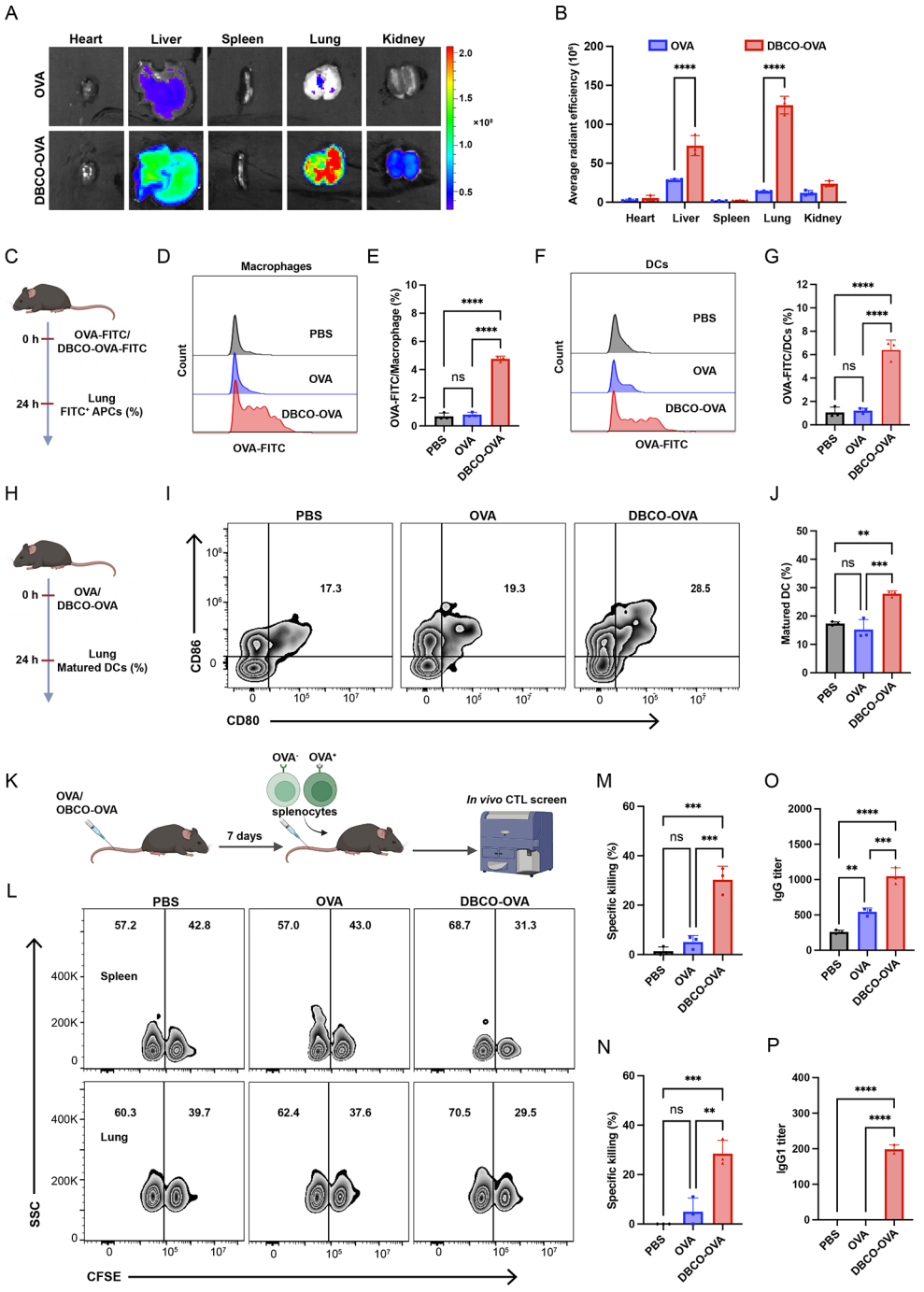


**Figure 4.** DBCO modification enhances the immunogenicity of protein vaccines *in vivo*. (A) *In vivo* fluorescence imaging showing organ-specific distribution of the OVA-FITC and DBCO-OVA-FITC in mice. (B) Quantification of fluorescence signals from *in vivo* imaging (two-way ANOVA)). (C) Schematic overview of antigen uptake analysis by pulmonary antigen-presenting cells. (D, E) Flow cytometry analysis of antigen uptake by pulmonary macrophages at 24 h following OVA-FITC or DBCO-OVA-FITC administration. (F, G) Flow cytometry analysis of antigen uptake by pulmonary DCs at 24 h following OVA-FITC or DBCO-OVA-FITC administration. (H) Schematic overview of DC maturation analysis in the lung. (I, J) Flow cytometry quantification of the percentages of mature pulmonary DCs ($CD80^+CD86^+$)/ $CD11c^+$ DCs following DBCO-OVA or OVA administration. (K) Schematic overview of *in vivo* CTL cytotoxicity assay. (L) Representative plots showing *in vivo* CTL cytotoxicity assay, demonstrating the enhanced cytotoxic response immunized with DBCO-OVA. (M) Quantification of antigen-specific cytotoxicity in the spleen. (N) Quantification of antigen-specific cytotoxicity in the lung. (O, P) ELISA detection of OVA-specific IgG and IgG1 antibody titers in serum 7 days after immunization with OVA or DBCO-OVA. *P* values in E, G, J, M, N, and P are analyzed using one-way ANOVA. The data are presented as mean ± SD. $n = 3$ mice/group. In A, representative images from three independent mice are shown. ns, no significance; $^*P < 0.05$; $^{**}P < 0.01$; $^{***}P < 0.001$; $^{****}P < 0.0001$. Panel C, H, and K created with BioRender.com.

In addition, Ki-67 immunofluorescence staining revealed a significant reduction in proliferation markers in tumors from the DBCO-TCL group, indicating an enhanced suppression of tumor cell proliferation (Figure 3I,J). DBCO-TCL treatment substantially elevated the proportions of MHC $II^+$ and $CD80^+CD86^+$ DCs in tumor tissue (Figure 3M−O).



https://doi.org/10.1021/jacs.5c17189
J. Am. Chem. Soc. 2026, 148, 8223−8235

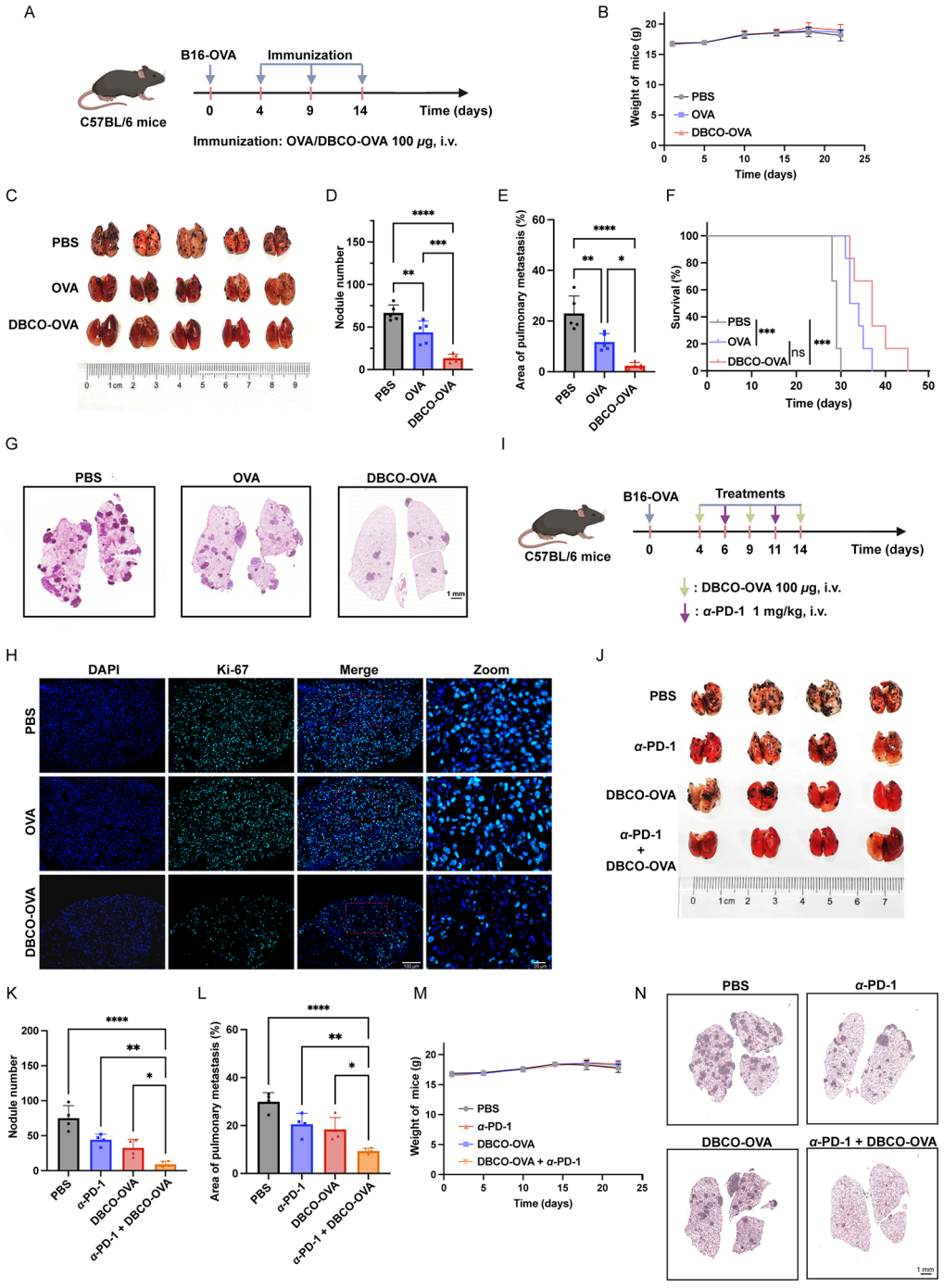


**Figure 5.** DBCO-OVA suppresses pulmonary metastasis. (A) Schematic of the treatment protocol for the B16-OVA lung metastasis model using DBCO-OVA. Mice were intravenous (i.v.) injected with B16-OVA cells and were i.v. injected with 100 mg of OVA or DBCO-OVA on days 4, 9, and 14 post-tumor inoculation. On day 22, lungs were collected for metastasis quantification. (B) Body weight monitoring during treatment ($n$ = 5 mice/group). (C) Images of dissected lungs from treated mice on day 22. (D) Quantification of pulmonary metastatic nodules. (E) Quantitative analysis of the average nodule sizes of pulmonary metastases. (F) Survival curves of the treated mice. (G) H&E staining of lung tissue. (H) Immunofluorescence staining of Ki-67 in the nodules of lung metastases. Bar = 100 $\mu$m. Zoom, ×5. (I) Schematic representation of the combination therapy protocol using DBCO-OVA and $\alpha$-PD-1. Mice were i.v. injected with B16-OVA cells and were i.v. injected with 100 mg of OVA or DBCO-OVA on days 4, 9, and 14, i.v. injected with $\alpha$-PD-1 (1 mg/kg) on days 6 and 11, post-tumor inoculation. On day 22, lungs were collected for metastasis quantification. (J) Images of dissected lungs after combination therapy ($n$ = 4 mice/group). (K) Quantification of pulmonary metastatic nodules after combination therapy. (L) Quantitative analysis of the average nodule sizes of pulmonary metastases after combination therapy. (M) Body weight changes during combination therapy. (N) H&E staining of lung tissue after combination therapy. $n$ = 4 mice/group. In (G, H, N), representative images from three independent mice are shown. Statistical analysis was performed using one-way ANOVA, and the data are presented as mean ± SD; ns, no significance; *$P$ < 0.05; **$P$ < 0.01; ***$P$ < 0.001; ****$P$ < 0.0001. Panels (A) and (I) created with BioRender.com.



https://doi.org/10.1021/jacs.5c17189
J. Am. Chem. Soc. 2026, 148, 8223−8235

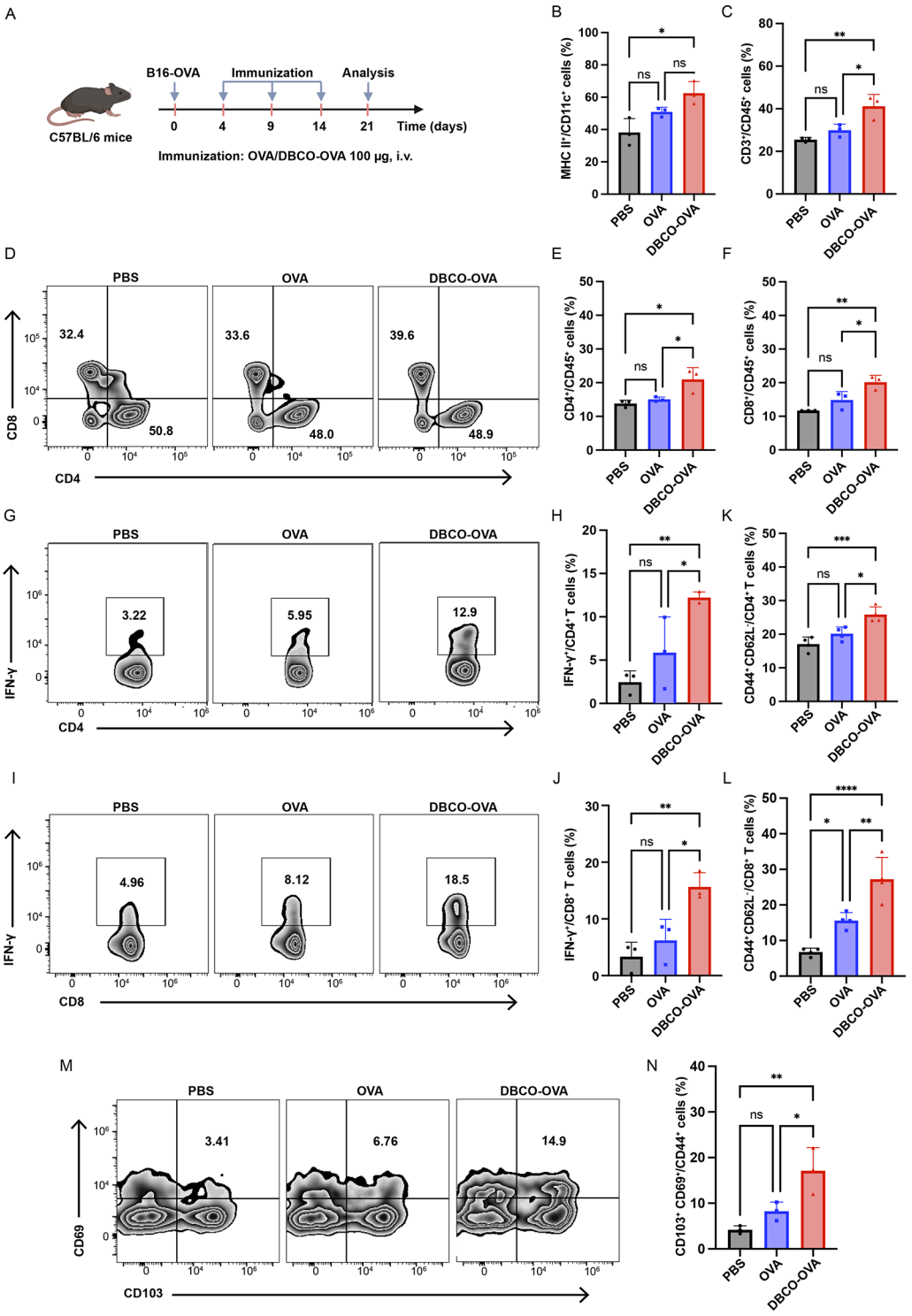


**Figure 6.** DBCO-OVA reprograms the pulmonary immune microenvironment. (A) Schematic of the DBCO-OVA treatment protocol in the B16-OVA lung metastasis model. C57BL/6 mice bearing B16-OVA lung metastases received i.v. DBCO-OVA or OVA (100 $\mu$g) as indicated on days 4, 9, and 14. On day 21, lungs were collected and analyzed by flow cytometry. (B) Quantification of the percentages of MHC II$^+$ cells in CD11c$^+$ cells. (C) Quantification of the percentages of CD3$^+$ T cells in CD45$^+$ cells. (D–F) Representative flow cytometry plots and quantification of the percentages of CD4$^+$ and CD8$^+$ T cells in CD45$^+$ cells in the lungs. (G, H) Representative flow cytometry plots and quantification of the percentages of IFN-$\gamma^+$ in CD4$^+$ T cells. (I, J) Representative flow cytometry plots and quantification of the percentages of IFN-$\gamma^+$ in CD8$^+$ T cells. (K, L) Quantification of the percentages of effector memory T cells (CD44$^+$CD62L$^-$) in CD4$^+$ or CD8$^+$ cells in the spleen. (M, N) Representative plots and quantification of the percentages of tissue-resident memory T cells (CD103$^+$CD69$^+$) in CD44$^+$CD8$^+$ T cells in lungs. $n$ = 3 mice/group. Statistical analysis was performed using one-way ANOVA, and the data are presented as mean ± SD; ns, no significance; *$P$ < 0.05; **$P$ < 0.01; ***$P$ < 0.001; ****$P$ < 0.0001. Panel A created with BioRender.com.



https://doi.org/10.1021/jacs.5c17189
J. Am. Chem. Soc. 2026, 148, 8223–8235

Concurrently, an increased $CD3^+$ T-cell infiltration was observed in the tumor microenvironment (Figure 3K,L), where $CD4^+$ T-cell numbers showed no statistical differences, and $CD8^+$ T cells were significantly augmented (Figure 3P,Q). Functional analysis revealed 2.7-fold and 1.5-fold increases in IFN-$\gamma$ and granzyme B expression, respectively, in $CD8^+$ T cells (Figure 3R−T), indicating that DBCO-TCL-pulsed DCs promote T-cell recruitment and activation. Furthermore, there were significantly higher proportions of both $CD4^+$ and $CD8^+$ effector memory T cells ($CD44^+CD62L^-$) in the DBCO-TCL group (Figure 3U,V), potentially enabling long-term antitumor immune memory. Thus, unlike traditional DBCO applications in click chemistry for bioconjugation, we explored DBCO as a direct antigen modifier or adjuvant to enhance DC-mediated antitumor immunity and not simply as a tool for linking molecules or modifying cell surfaces.

## DBCO-Antigen Vaccine Boosts Systemic Immune Activation

To further assess the immune-activating and antitumor potential of DBCO-conjugated vaccines, we first characterized the biodistribution of DBCO-conjugated antigens *in vivo*. We intravenously injected FITC-labeled unmodified OVA and DBCO-OVA into mice, followed by fluorescence imaging at 8 h postinjection. DBCO-OVA exhibited significantly prolonged systemic retention and lung-specific accumulation compared to unmodified OVA, as indicated by stronger fluorescent signals in pulmonary regions (Figure 4A).

Quantification revealed an 8.9-fold higher lung fluorescence intensity, highlighting the lung-targeting capability conferred by DBCO-modified OVA (Figure 4B). To determine whether DBCO modification improves antigen uptake by pulmonary APCs, we performed a quantitative flow cytometry analysis of alveolar macrophages (AMs) and pulmonary DCs (Figure 4C). Results showed that DBCO-OVA significantly enhanced antigen uptake, with a 5.9-fold increase in AMs and a 5.3-fold increase in pulmonary DCs compared to the unmodified group (Figure 4D−G). Moreover, DBCO modification promoted DC maturation and activation in the lungs, as evidenced by an increase in the proportion of $CD80^+CD86^+$ double-positive DCs from 15.2 to 27.9% (Figure 4H−J). Next, the OVA-specific CTL response was quantified by adoptive transfer of CFSE-labeled splenocytes (Figure 4K). Results indicated that DBCO-OVA treatment induced stronger CTL activity in both spleen and lung tissues, with killing efficiencies reaching 27.3 ± 8 and 28.5 ± 5.4%, representing 7.1-fold and 6.5-fold increases, respectively, compared to unmodified OVA (Figure 4L−N). These findings suggest that DBCO modification enhances the MHC I cross-presentation and CTL activation. Additionally, DBCO-OVA also augmented the humoral immune responses. Total IgG titers were increased from 544.7 ± 54.3 to 1048.2 ± 119.8 (1.9-fold, Figure 4O), while the IgG1 subtype—barely detectable in the unmodified group—showed a significant expression (198.6 ± 12.0, Figure 4P) in the DBCO-OVA group, indicating Th2-associated antibody response potentiation. Crucially, to rule out immunogenicity against the DBCO moiety itself, we further measured the DBCO-specific antibody titers. As shown in Figure S9, the levels of DBCO-specific IgG and IgM in the DBCO-OVA group were statistically indistinguishable from those in the PBS and unmodified OVA control groups. These findings demonstrate that DBCO modification successfully directed the adaptive immune response toward the protein antigen without inducing off-target immunity against the chemical linker.

In summary, modification of DBCO to antigen substantially improves the retention of protein antigens, enhances pulmonary APC uptake capacity, and comprehensively elevates vaccine immunogenicity through activation of cellular and humoral immunity.

## DBCO-Antigen Vaccine Suppresses Lung Metastasis and Reshapes the Metastatic Microenvironment

To evaluate DBCO-OVA's therapeutic potential in lung metastasis, we established a B16-OVA metastasis model in mice and administered three injections to demonstrate that DBCO modification successfully directed the adaptivections of PBS, OVA, or DBCO-OVA vaccines (100 $\mu$g/injection) according to the schedule shown in Figure 5A. All groups maintained stable body weights, indicating vaccine safety (Figure 5B). On day 22, mice were euthanized for lung tissue analysis. Macroscopic examination revealed a significant reduction in visible metastatic nodules in the DBCO-OVA group (Figure 5C). Quantitative analysis showed a 69.4% reduction in lung nodule counts compared with the OVA group and a 79.3% reduction compared with the PBS control (Figure 5D). Quantitative analysis of the area also demonstrated that DBCO-OVA exhibited a marked inhibitory effect on pulmonary metastasis (Figure 5E). Survival analysis showed that the median survival in the DBCO-OVA group extended to 37 days compared to 29 days in the PBS group (Figure 5F). While the difference between the DBCO-OVA and OVA groups was not statistically significant, a trend toward prolonged survival was observed. Histological analysis further confirmed these findings as there was reduced tumor infiltration and the best-preserved alveolar structure in the DBCO-OVA group (Figure 5G). In addition, Ki-67 staining demonstrated that DBCO-OVA significantly suppressed tumor cell proliferation (Figure 5H). Next, we combined the DBCO-OVA vaccine with the immune checkpoint inhibitor $\alpha$-PD-1 antibody to evaluate their combined antitumor effects (Figure 5I). Quantification of lung metastatic nodules showed that the combination therapy group exhibited a significant reduction in tumor burden compared with either monotherapy treatment, achieving an inhibition rate exceeding 72.3% (Figure 5J−L). No significant weight loss or observable toxicity was noted during treatment, indicating that the combined strategy was well tolerated (Figure 5M). Histological analysis further confirmed that there was minimal tumor infiltration and the best-preserved alveolar structure in the combination group (Figure 5N). These results suggest that DBCO-OVA vaccination enhances the therapeutic efficacy of the $\alpha$-PD-1 blockade in suppressing lung metastases.

To understand how the DBCO-antigen vaccine triggers immune responses against lung metastasis, we performed a comprehensive analysis of immune cell composition and functional status in lung tissue and spleen using multi-parameter flow cytometry with a focus on APCs, effector T cells, and memory T-cell subsets (Figure 6A). In the lung tissue, the expression level of MHC II on $CD11c^+$ DCs was significantly increased to 62.5 ± 7.1% in the DBCO-OVA-treated group, approximately 1.6-fold higher than that in the PBS group (Figure 6B). The DBCO-OVA group also exhibited enhanced T-cell infiltration, with $CD3^+$ T cells accounting for 41.1% of lung immune cell infiltration. Among them, $CD4^+$ and $CD8^+$ T-cell subpopulations increased to 20.9 and 20.2%,


https://doi.org/10.1021/jacs.5c17189
J. Am. Chem. Soc. 2026, 148, 8223−8235

respectively, representing ∼1.5-fold and ∼1.7-fold increases compared to the PBS group (Figure 6C−F). Further analysis revealed that the DBCO-OVA vaccine significantly enhanced T-cell effector activity in the lung metastatic microenvironment. The proportion of IFN-$\gamma^+$ $CD4^+$ T cells reached 12.2 ± 0.6%, representing 5.0-fold and 2.1-fold increases compared to the PBS and OVA groups, respectively (Figure 6G,H). IFN-$\gamma^+$ $CD8^+$ T cells increased to 15.6 ± 2.5%, approximately 4.7-fold and 2.5-fold increases over the PBS and OVA groups, respectively (Figure 6I,J). These results demonstrate that the DBCO-antigen vaccine effectively remodels the pulmonary immune microenvironment by promoting DC activation and T-cell infiltration, thereby improving antitumor immune responses.

To assess the induction of long-term immune protection, we further analyzed systemic effector memory T cells (TEM) and tissue-resident memory T cells (TRM). Flow cytometry showed that the DBCO-OVA vaccine significantly expanded splenic TEM populations, with $CD4^+$ TEM ($CD4^+CD44^+CD62L^-$) cells accounting for 25.8 ± 2.5% in $CD4^+$ T cells and $CD8^+$ TEM ($CD8^+CD44^+CD62L^-$) cells reaching 27.3 ± 6.2% in $CD8^+$ T cells (Figure 6K,L). Meanwhile, $CD8^+$ TRM ($CD44^+CD103^+CD69^+$) cells in the lung tissues increased to 17.1 ± 5.1% in $CD44^+CD8^+$ T cells, showing 4.1-fold and 2.1-fold increases over PBS and the OVA groups (Figure 6M,N). These findings indicate that the DBCO-antigen vaccine elicits both local immune residency and systemic memory responses, establishing a coordinated local-systemic immune defense against cancer.

### Biosafety Evaluation of DBCO-OVA Treatment

To assess the *in vivo* biosafety of the DBCO-modified vaccine, we conducted a comprehensive evaluation of the systemic toxicity and inflammatory responses. Serum biochemical markers of liver, kidney, and cardiac function were first analyzed. As shown in Figure A10A,H, mice treated with DBCO-OVA exhibited levels of alanine aminotransferase (ALT), aspartate aminotransferase (AST), total bilirubin (TBIL), creatinine (CREA), urea (UREA), creatine kinase (CK), and creatine kinase-MB (CK-MB) that were statistically indistinguishable from those observed in the PBS control group, indicating no detectable functional impairment of major organs. To further assess the risk of systemic inflammatory responses, serum levels of the pro-inflammatory cytokines IL-6 and TNF-$\alpha$ were measured. No significant elevation of either cytokine was detected following vaccination (Figure S10I,J). In addition, to evaluate potential autoimmune induction, sera from vaccinated mice were screened for antinuclear antibodies (ANA) and anti-Smith (anti-Sm) antibodies. As shown in Tables S2 and S3, all mice in the DBCO-OVA group tested negative for both ANA and anti-Sm, comparable to the PBS control group.

Finally, histological examination of major organs, including the heart, liver, spleen, lung, and kidney, revealed normal tissue architecture with no signs of pathological damage (Figure S10K). Collectively, these data provide an initial biosafety assessment of the DBCO-OVA vaccine and indicate a favorable biocompatibility profile under the experimental conditions tested.

## DISCUSSION

Therapeutic cancer vaccines have long promised to induce robust and specific antitumor immunity, yet their clinical impact has been hindered due to inefficient antigen delivery, poor immunogenicity, and ineffective APC activation. In this study, we present a streamlined, chemistry-based antigen modification strategy using DBCO, which enhances cancer vaccine performance while maintaining biocompatibility.

We demonstrate that direct DBCO conjugation to protein antigens improves their biodistribution and uptake by APCs. Compared to prior DBCO-related cancer vaccine studies, which employ DBCO for nanoparticle cross-linking or cell surface engineering,[19,20] our work uniquely reports that DBCO modification to antigen can enhance vaccine efficacy. We successfully modified various antigens, including a model antigen and tumor cell lysates, with DBCO, demonstrating the flexibility and broad applicability of this strategy. Mechanistically, DBCO modification enhanced DC function via the NF-$\kappa$B/iNOS signaling axis and collectively promoted both cytotoxic T-cell responses and antibody production, translating into improved therapeutic efficacy against lung metastases in a murine melanoma model. Notably, DBCO-OVA vaccination reshaped the tumor microenvironment by promoting DC activation, effector T-cell infiltration, and functional reprogramming, while also contributing to a sustained antitumor immune network via systemic and tissue-resident memory T-cell expansion. When combined with the PD-1 blockade, the modified vaccine further enhanced therapeutic responses, underscoring its compatibility with current immunotherapies.

To bridge the gap between model antigens and clinically relevant tumor antigens, we evaluated the DBCO conjugation strategy using B16-F10 tumor cell lysates. Unlike single-epitope vaccines, whole tumor cell lysates provide a heterogeneous antigenic repertoire that better reflects the tumor complexity and antigenic diversity. DBCO modification again enhanced the immunogenicity of tumor-lysate-based vaccines and improved tumor control. While tumor lysates lack the precision of defined neoantigen vaccines, these results suggest the feasibility of extending the DBCO strategy to complex, multiepitope antigen formulations. Building on these findings, future studies applying this approach to sequence-validated neoantigens may further refine antigen specificity and enable evaluation in more precise and personalized cancer vaccine settings.

This work demonstrates the potential of rational chemical conjugation to modulate antigen pharmacokinetics and immune engagement without the need for complex delivery systems. The modularity and simplicity of DBCO conjugation offer a versatile platform for tailoring protein vaccines against diverse tumor antigens and metastatic niches. Future studies leveraging this strategy with clinically relevant neoantigens, multiepitope constructs, or personalized tumor antigens could accelerate progress toward effective, scalable therapeutic cancer vaccines.

## ASSOCIATED CONTENT

### Supporting Information

The Supporting Information is available free of charge at https://pubs.acs.org/doi/10.1021/jacs.5c17189.

Experimental details, synthesis procedures, characterization of THDBCO-$PEG_4$-NHS, and *in vitro* and *in vivo* evaluation (PDF)

LC-MS/MS result of BDCO-OVA (XLSX)



https://doi.org/10.1021/jacs.5c17189
J. Am. Chem. Soc. 2026, 148, 8223−8235

## AUTHOR INFORMATION


### Corresponding Authors

**Jianjun Cheng** − *School of Engineering and School of Engineering and Research Center for Industries of the Future, Westlake University, Hangzhou 310030, China; Institute of Advanced Technology, Westlake Institute for Advanced Study, Hangzhou 310024, China;* orcid.org/0000-0003-2561-9291; Email: chengjianjun@westlake.edu.cn

**Minmin Xiong** − *Biotherapy Center, Sun Yat-Sen Memorial Hospital, Sun Yat-Sen University, Guangzhou 510120, China*; Email: xiongmm5@mail.sysu.edu.cn

**Kaiting Yang** − *School of Biomedical Sciences and Engineering, South China University of Technology, Guangzhou International Campus, Guangzhou 511442, China; National Engineering Research Centre for Tissue Restoration and Reconstruction, South China University of Technology, Guangzhou 510006, China*; Email: yangkt@scut.edu.cn

**Yan Bao** − *Guangdong Provincial Key Laboratory of Malignant Tumor Epigenetics and Gene Regulation, Sun Yat-Sen Memorial Hospital, Sun Yat-Sen University, Guangzhou 510120, China; Nanhai Translational Innovation Center of Precision Immunology, Sun Yat-Sen Memorial Hospital, Foshan 528200, China;* orcid.org/0000-0002-5072-9428; Email: baoy5@mail.sysu.edu.cn

### Authors

**Zhiguo Li** − *Guangdong Provincial Key Laboratory of Malignant Tumor Epigenetics and Gene Regulation, Sun Yat-Sen Memorial Hospital and Breast Tumor Center, Sun Yat-sen Memorial Hospital, Sun Yat-Sen University, Guangzhou 510120, China*

**Tengyao Wang** − *Guangdong Provincial Key Laboratory of Malignant Tumor Epigenetics and Gene Regulation, Sun Yat-Sen Memorial Hospital and Biotherapy Center, Sun Yat-Sen Memorial Hospital, Sun Yat-Sen University, Guangzhou 510120, China*

**Weifan Li** − *Guangdong Provincial Key Laboratory of Malignant Tumor Epigenetics and Gene Regulation, Sun Yat-Sen Memorial Hospital and Biotherapy Center, Sun Yat-Sen Memorial Hospital, Sun Yat-Sen University, Guangzhou 510120, China*

**Peiyu Yu** − *Department of Chemistry, School of Science, Westlake University, Hangzhou 310030, China*

**Kangxiu Wu** − *Department of Clinical Laboratory, Sun Yat-sen Memorial Hospital, Sun Yat-Sen University, Guangzhou 510120, China*

**Chanjuan Su** − *Guangdong Provincial Key Laboratory of Malignant Tumor Epigenetics and Gene Regulation, Sun Yat-Sen Memorial Hospital, Sun Yat-Sen University, Guangzhou 510120, China*

**Fuxiang Wang** − *Guangdong Provincial Key Laboratory of Malignant Tumor Epigenetics and Gene Regulation, Sun Yat-Sen Memorial Hospital, Sun Yat-Sen University, Guangzhou 510120, China*

**Huosheng Zhou** − *Guangdong Provincial Key Laboratory of Malignant Tumor Epigenetics and Gene Regulation, Sun Yat-Sen Memorial Hospital, Sun Yat-Sen University, Guangzhou 510120, China*

**Fan Lan** − *Guangdong Provincial Key Laboratory of Malignant Tumor Epigenetics and Gene Regulation, Sun Yat-Sen Memorial Hospital, Sun Yat-Sen University, Guangzhou 510120, China*

**Yaofeng Zhou** − *School of Engineering, Westlake University, Hangzhou 310030, China; Institute of Advanced Technology, Westlake Institute for Advanced Study, Hangzhou 310024, China*

**Kaimin Cai** − *Surio Therapeutics Co., Ltd, Hangzhou 310012, China*

**Menghua Xiong** − *School of Biomedical Sciences and Engineering, South China University of Technology, Guangzhou International Campus, Guangzhou 511442, China; National Engineering Research Centre for Tissue Restoration and Reconstruction, South China University of Technology, Guangzhou 510006, China;* orcid.org/0000-0003-0020-5965

**Songyin Huang** − *Biotherapy Center, Sun Yat-Sen Memorial Hospital, Sun Yat-Sen University, Guangzhou 510120, China; Guangdong Provincial Key Laboratory of Cancer Pathogenesis and Precision Diagnosis and Treatment, Shenshan Medical Center, Sun Yat-sen Memorial Hospital, Sun Yat-Sen University, Shanwei 516621, China*

Complete contact information is available at: https://pubs.acs.org/10.1021/jacs.5c17189

### Author Contributions

§Z.L., T.W., and W.L. contributed equally to this work.


### Notes

The authors declare the following competing financial interest(s): Yan Bao, Songyin Huang, Zhiguo Li and Tengyao Wang have submitted a patent application (2025117127135) related to this study.

## ACKNOWLEDGMENTS

The authors thank the financial support from the "Pioneer" and "Leading Goose" R&D Program of Zhejiang (2024SDXHDX 0004), the National Natural Science Foundation of China (32522050, 82471873, 82300586, and 82371856), the Guangdong Basic and Applied Basic Research Foundation (2023B1515020086 and 2025A1515010100), the Foundation of Guangdong Science and Technology Department (2024B1212030002), the Foundation of Guangzhou Science and Technology Bureau (2024A03J1055 and 2025A03J4194), and the Sun Yat-sen Pilot Scientific Research Fund (YXQH202307). The table of contents graphic and Figures 1Z, 3A,E, 4C,H,K, 5A,I, and 6A and Figure S10 were created with BioRender.com.

## REFERENCES

(1) Braun, D. A.; Moranzoni, G.; Chea, V.; McGregor, B. A.; Blass, E.; Tu, C. R.; Vanasse, A. P.; Forman, C.; Forman, J.; Afeyan, A. B.; Schindler, N. R.; Liu, Y.; Li, S.; Southard, J.; Chang, S. L.; Hirsch, M. S.; LeBoeuf, N. R.; Olive, O.; Mehndiratta, A.; Greenslade, H.; Shetty, K.; Klaeger, S.; Sarkizova, S.; Pedersen, C. B.; Mossanen, M.; Carulli, I.; Tarren, A.; Duke-Cohan, J.; Howard, A. A.; Iorgulescu, J. B.; Shim, B.; Simon, J. M.; Signoretti, S.; Aster, J. C.; Elagina, L.; Carr, S. A.; Leshchiner, I.; Getz, G.; Gabriel, S.; Hacohen, N.; Olsen, L. R.; Oliveira, G.; Neuberg, D. S.; Livak, K. J.; Shukla, S. A.; Fritsch, E. F.; Wu, C. J.; Keskin, D. B.; Ott, P. A.; Choueiri, T. K. A Neoantigen Vaccine Generates Antitumour Immunity in Renal Cell Carcinoma. *Nature* **2025**, *639* (8054), 474−482.

(2) Jiang, T.; Shi, T.; Zhang, H.; Hu, J.; Song, Y.; Wei, J.; Ren, S.; Zhou, C. Tumor Neoantigens: From Basic Research to Clinical Applications. *J. Hematol Oncol* **2019**, *12* (1), 93.

(3) Luri-Rey, C.; Teijeira, Á.; Wculek, S. K.; De Andrea, C.; Herrero, C.; Lopez-Janeiro, A.; Rodríguez-Ruiz, M. E.; Heras, I.;

Aggelakopoulou, M.; Berraondo, P.; Sancho, D.; Melero, I. Cross-Priming in Cancer Immunology and Immunotherapy. *Nat. Rev. Cancer* **2025**, *25* (4), 249−273.
(4) Hou, Y.; Chen, M.; Bian, Y.; Zheng, X.; Tong, R.; Sun, X. Advanced Subunit Vaccine Delivery Technologies: From Vaccine Cascade Obstacles to Design Strategies. *Acta Pharm. Sin B* **2023**, *13* (8), 3321−3338.
(5) Grotzke, J. E.; Kozik, P.; Morel, J. D.; Impens, F.; Pietrosemoli, N.; Cresswell, P.; Amigorena, S.; Demangel, C. Sec61 Blockade by Mycolactone Inhibits Antigen Cross-Presentation Independently of Endosome-to-Cytosol Export. *Proc. Natl. Acad. Sci. U. S. A.* **2017**, *114* (29), E5910−E5919.
(6) Pardoll, D. M. The Blockade of Immune Checkpoints in Cancer Immunotherapy. *Nat. Rev. Cancer* **2012**, *12* (4), 252−264.
(7) Villadangos, J. A.; Schnorrer, P. Intrinsic and Cooperative Antigen-Presenting Functions of Dendritic-Cell Subsets in Vivo. *Nat. Rev. Immunol* **2007**, *7* (7), 543−555.
(8) Banchereau, J.; Steinman, R. M. Dendritic Cells and the Control of Immunity. *Nature* **1998**, *392* (6673), 245−252.
(9) Wculek, S. K.; Cueto, F. J.; Mujal, A. M.; Melero, I.; Krummel, M. F.; Sancho, D. Dendritic Cells in Cancer Immunology and Immunotherapy. *Nat. Rev. Immunol* **2020**, *20* (1), 7−24.
(10) Zhang, T.; He, P.; Guo, D.; Chen, K.; Hu, Z.; Zou, Y. Research Progress of Aluminum Phosphate Adjuvants and Their Action Mechanisms. *Pharmaceutics* **2023**, *15* (6), 1756.
(11) O'Hagan, D. T.; van der Most, R.; Lodaya, R. N.; Coccia, M.; Lofano, G. World in Motion" - Emulsion Adjuvants Rising to Meet the Pandemic Challenges. *NPJ. Vaccines* **2021**, *6* (1), 158.
(12) Shi, S.; Zhu, H.; Xia, X.; Liang, Z.; Ma, X.; Sun, B. Vaccine Adjuvants: Understanding the Structure and Mechanism of Adjuvanticity. *Vaccine* **2019**, *37* (24), 3167−3178.
(13) Fortier, M. E.; Kent, S.; Ashdown, H.; Poole, S.; Boksa, P.; Luheshi, G. N. The Viral Mimic, Polyinosinic:Polycytidylic Acid, Induces Fever in Rats via an Interleukin-1-Dependent Mechanism. *Am. J. Physiol Regul Integr Comp Physiol* **2004**, *287* (4), R759−766.
(14) Cunningham, C.; Campion, S.; Teeling, J.; Felton, L.; Perry, V. H. The Sickness Behaviour and CNS Inflammatory Mediator Profile Induced by Systemic Challenge of Mice with Synthetic Double-Stranded RNA (Poly I:C). *Brain Behav Immun* **2007**, *21* (4), 490−502.
(15) Vasilakos, J. P.; Tomai, M. A. The Use of Toll-like Receptor 7/8 Agonists as Vaccine Adjuvants. *Expert Rev. Vaccines* **2013**, *12* (7), 809−819.
(16) Wang, H.; Mooney, D. J. Metabolic Glycan Labelling for Cancer-Targeted Therapy. *Nat. Chem.* **2020**, *12* (12), 1102−1114.
(17) Chang, P. V.; Prescher, J. A.; Sletten, E. M.; Baskin, J. M.; Miller, I. A.; Agard, N. J.; Lo, A.; Bertozzi, C. R. Copper-Free Click Chemistry in Living Animals. *Proc. Natl. Acad. Sci. U. S. A.* **2010**, *107* (5), 1821−1826.
(18) Agatemor, C.; Buettner, M. J.; Ariss, R.; Muthiah, K.; Saeui, C. T.; Yarema, K. J. Exploiting Metabolic Glycoengineering to Advance Healthcare. *Nat. Rev. Chem.* **2019**, *3* (10), 605−620.
(19) Stickdorn, J.; Stein, L.; Arnold-Schild, D.; Hahlbrock, J.; Medina-Montano, C.; Bartneck, J.; Ziß, T.; Montermann, E.; Kappel, C.; Hobernik, D.; Haist, M.; Yurugi, H.; Raabe, M.; Best, A.; Rajalingam, K.; Radsak, M. P.; David, S. A.; Koynov, K.; Bros, M.; Grabbe, S.; Schild, H.; Nuhn, L. Systemically Administered TLR7/8 Agonist and Antigen-Conjugated Nanogels Govern Immune Responses against Tumors. *ACS Nano* **2022**, *16* (3), 4426−4443.
(20) Yang, H.; Xiong, Z.; Heng, X.; Niu, X.; Wang, Y.; Yao, L.; Sun, L.; Liu, Z.; Chen, H. Click-Chemistry-Mediated Cell Membrane Glycopolymer Engineering to Potentiate Dendritic Cell Vaccines. *Angew. Chem. Int. Ed* **2024**, *63* (2), No. e202315782.
(21) Guo, Q.; Jin, Y.; Chen, X.; Ye, X.; Shen, X.; Lin, M.; Zeng, C.; Zhou, T.; Zhang, J. NF-κB in Biology and Targeted Therapy: New Insights and Translational Implications. *Signal Transduct. Target Ther.* **2024**, *9* (1), 53.
(22) Tang, F.; Zhang, J. N.; Xu, L. Y.; Zhao, X. L.; Wan, F.; Ao, H.; Peng, C. Endothelial-Derived Exosomes: A Novel Therapeutic Strategy for LPS-Induced Myocardial Damage with Anisodamine. *Int. J. Biol. Macromol.* **2024**, *282*, No. 136993.
(23) Yang, L.; Cao, L.; Li, C.; Li, X.; Wang, J.; Chen, H.; He, J. Hostaflavone A from Hosta Plantaginea (Lam.) Asch. Blocked NF-κB/iNOS/COX-2/MAPKs/Akt Signaling Pathways in LPS-Induced RAW 264.7 Macrophages. *Journal of Ethnopharmacology* **2022**, *282*, No. 114605.
(24) Ghasemi-Dehnoo, M.; Amini-Khoei, H.; Lorigooini, Z.; AnjomShoa, M.; Rafieian-Kopaei, M. Ferulic Acid Ameliorates Ulcerative Colitis in a Rat Model via the Inhibition of Two LPS-TLR4-NF-κB and NF-κB-INOS-NO Signaling Pathways and Thus Alleviating the Inflammatory, Oxidative and Apoptotic Conditions in the Colon Tissue. *Inflammopharmacol* **2023**, *31* (5), 2587−2597.




https://doi.org/10.1021/jacs.5c17189
J. Am. Chem. Soc. 2026, 148, 8223−8235